

these metals. By choice of metal and fluorophore, it is also possible to "hide" the barcode pattern in fluorescence images.

As interest grows in carrying out comprehensive analyses on classes of biologically relevant molecules (e.g., genomics, proteomics, metabolomics), there is a demand for very high-level multiplexing in small sample volumes, and thus a corresponding need for new readout mechanisms. Solution arrays of highly encodable and chemically diverse nanoparticles, such as those described herein, offer an intriguing solution to both requirements.

References and Notes

1. D. J. Harrison *et al.*, *Science* **261**, 895 (1993).
2. V. G. Cheung *et al.*, *Nature Genet. Suppl.* **21**, 15 (1999).
3. M. R. Henry, P. Wilkins Stevens, J. Sun, D. M. Kelso, *Anal. Biochem.* **276**, 204 (1999).
4. S. A. Dunbar, J. W. Jacobson, *Clin. Chem.* **46**, 1498 (2000).
5. D. R. Walt, *Science* **287**, 451 (2000).
6. B. J. Battersby *et al.*, *J. Am. Chem. Soc.* **122**, 2138 (2000).
7. M. Han, X. Gao, J. Z. Su, S. Nie, *Nature Biotechnol.* **19**, 631 (2001).
8. D. Almalawi, C. Z. Liu, M. Moskovits, *J. Mater. Res.* **9**, 1014 (1994).
9. J. C. Hulteen, C. R. Martin, *J. Mater. Chem.* **7**, 1075 (1997).
10. B. R. Martin *et al.*, *Adv. Mater.* **11**, 1021 (1999).
11. The membranes used in this work are Al₂O₃ and have a nominal pore diameter of 200 nm. However, the pores are 200 nm only at the surface of the membrane. SEM measurements indicate that the pores widen to ~400 nm in the central region of the membrane, with an average diameter of 318 ± 50 nm. All of the particles discussed in this report have diameters in this range [as determined by transmission electron microscopy (TEM) and SEM].
12. T. A. Savas, M. L. Schattenburg, J. M. Carter, H. I. Smith, *J. Vac. Sci. Technol. B* **14**, 4167 (1996).
13. T. Thurn-Albrecht *et al.*, *Science* **290**, 2126 (2000).
14. H. Masuda *et al.*, *Adv. Mater.* **13**, 189 (2001).
15. K. C. Grabar *et al.*, *Anal. Chem.* **69**, 471 (1997).
16. Particles were characterized electrochemically during the deposition process. After preparation, they were characterized by the following techniques: TEM, SEM, FE-SEM, energy-dispersive x-ray scattering, macroscopic extinction, microscopic reflectivity, atomic absorption, and chemical treatment (e.g., selective dissolution of less noble segments).
17. D. R. Lide, *CRC Handbook of Chemistry and Physics* (CRC Press, Cleveland, OH, ed. 71, 1990), pp. 12-87-12-102.
18. S. Inoue, K. R. Spring, *Video Microscopy* (Plenum, New York, ed. 2, 1997).
19. The equation for calculation of unique sequences for a barcode of *n* metals and *s* stripes is *n^s* for particles read in only one direction (i.e., having "start" markers), and $[n^s + n^{ceil(s/2)}]/2$ for particles read randomly in either direction (20). Thus, for a 6.5-μm particle comprising 500-nm stripes of two different metals, use of a 500-nm "start" marker gives 2¹² = 4096, whereas a 13-segment particle with no "start" marker gives $(2^{13} + 2^7)/2 = 4160$.
20. The formula for the case with two different metals is described in N. Hoffman, *2-Year Coll. Math. J.* **9**, 267 (1978). For the more general case, see www.research.att.com/~njas/sequences/transforms2.html.
21. M. Bruchez Jr., M. Moronne, P. Gin, S. Weiss, A. P. Alivisatos, *Science* **281**, 2013 (1998).
22. W. C. W. Chan, S. Nie, *Science* **281**, 2016 (1998).
23. In practice, the striping pattern can be combined with different particle lengths and stripe compositions to yield either a greater total number of distinctive patterns or, perhaps more important, a set of parti-

- cles selected for ease of identification (i.e., by computer software).
24. More than 95% of all 1× segments will be shorter than 500 nm + 2(10%) = 600 nm, and >95% of all 2× segments will be longer than 1000 nm - 2(10%) = 800 nm (25). For 350-nm segments, >95% of all 1× segments will be <420 nm, whereas 95% of all 2× segments will be >560 nm. Although the differences in these two lengths cannot be directly measured by optical microscopy, they should be distinguishable by differences in intensity. Note that we have prepared 230-nm stripes with 16% standard deviation, and we routinely prepare particles in the 4- to 8-μm range with <10% standard deviations in total length.
25. D. A. Skoog, D. M. West, F. J. Holler, *Fundamentals of Analytical Chemistry* (Saunders, New York, ed. 6, 1992), p. 42.
26. A. Ulman, *An Introduction to Ultrathin Films from Langmuir-Blodgett to Self-Assembly* (Academic Press, New York, 1991).
27. P. Harder, M. Grunze, G. M. Whitesides, P. E. Laibinis, *J. Phys. Chem. B* **102**, 426 (1998).
28. DNA sequences: (a) "capture" oligonucleotide: 5'-biotin-AAAAAAGCGATTCCAGGAT-3', (b) analyte: 5'-TACGAGTTGAGAATCTCGAATCGG-3', (c) "detection" oligonucleotide: 5'-TCTCAACTCGTA-fluor-3', where fluor = tetramethylrhodamine (TAMRA).
29. Particles were first derivatized with NeutrAvidin (0.1 mg/ml, Pierce) by adsorption of the protein to the surface for 1 hour in 0.3 M phosphate-buffered saline (PBS, pH 7.0). This was followed by attachment of a biotinylated capture 12-nucleotide oligomer, **a**. The sample was prehybridized with a solution of 0.1% SDS in 0.3 M PBS for 15 min. The analyte, **b**, a 24-nucleotide oligomer (4 μM) was hybridized with **a** for 2 hours by

- heating to 60°C with passive cooling to room temperature in the water bath. The samples were rinsed and detection proceeded by hybridization with a TAMRA-labeled detection oligomer, **c** (4 μM), for 2 hours at 30°C. After hybridization, the samples were rinsed first with 1% SDS in 0.3 M PBS, then with 0.1% SDS in 0.3 M PBS, and finally with 0.3 M PBS.
30. Particles were derivatized with 16-mercaptohexadecanoic acid to which the capture antibody, **a**, was covalently attached using standard carbodiimide chemistry. For this assay, Au-Ag-Au rods were derivatized with antibody to human IgG (Fc specific), and Au-Ni-Au rods were derivatized with antibody to rabbit IgG (Fc specific). After attachment of the capture antibody, the rods were further derivatized with poly(ethylene glycol) (PEG) using a 1% solution of bis-aminated PEG. Non-specific sites on the capture antibody were blocked using a 1% solution of bovine serum albumin (BSA) in 0.3 M PBS (pH 7.0). The analytes, **b**, in this case human IgG and rabbit IgG, were mixed together to a final concentration of 0.05 mg/ml, added to a mixture of derivatized barcoded rods, and allowed to incubate for 30 min. After incubation, the sample was rinsed several times in 0.3 M PBS (pH 7.0) buffer and then incubated for an additional 30 min with a mixture of the detection antibodies, **c** [antibody to rabbit IgG (heavy and light chains) labeled with Texas Red; antibody to human IgG (γ specific) labeled with fluorescein isothiocyanate (FITC)]. After incubation with **c**, the sample was rinsed several times in buffer.
31. We thank T. Carado, P. Smith, W. Stonas, K. Shale, S. Norton, and L. Dietz for their help with particle synthesis and optical characterization. Supported by NIH grant HG02228 (C.D.K.).

30 May 2001; accepted 14 August 2001

Deposition of Conformal Copper and Nickel Films from Supercritical Carbon Dioxide

Jason M. Blackburn, David P. Long, Albertina Cabañas, James J. Watkins*

Device-quality copper and nickel films were deposited onto planar and etched silicon substrates by the reduction of soluble organometallic compounds with hydrogen in a supercritical carbon dioxide solution. Exceptional step coverage on complex surfaces and complete filling of high-aspect-ratio features of less than 100 nanometers width were achieved. Nickel was deposited at 60°C by the reduction of bis(cyclopentadienyl)nickel and copper was deposited from either copper(I) or copper(II) compounds onto the native oxide of silicon or metal nitrides with seed layers at temperatures up to 200°C and directly on each surface at temperatures above 250°C. The latter approach provides a single-step means for achieving high-aspect-ratio feature fill necessary for copper interconnect structures in future generations of integrated circuits.

The increasing complexity and decreasing dimensions of devices for microelectronic, system-on-a-chip, data storage, and other applications are placing stringent demands on deposition technologies that, to date, have not been fully satisfied. These include reductions in the thermal budget during fabrication, mitigation of the negative environmental impact

of current processes, conformal coverage of complex surfaces, and complete filling of narrow, high-aspect-ratio structures (1). The difficulties associated with achieving the latter two requirements are particularly severe. For example, to keep pace with the historical increase in processor speed popularly referred to as Moore's Law, Cu interconnect structures for integrated circuits must drop below 100 nm in width with aspect ratios that exceed 3 after 2005. According to the Semiconductor Industry Association's International Technology Roadmap for Semiconductors

Department of Chemical Engineering, University of Massachusetts, Amherst, MA 01003, USA.

*To whom correspondence should be addressed. E-mail: watkins@ecs.umass.edu

REPORTS

(ITRS), however, there are no viable means for Cu deposition at these dimensions (1).

We have developed a technique, called chemical fluid deposition (CFD), that can meet each of the criteria outlined above, for interconnect technology in particular, and device fabrication in general. CFD involves the chemical reduction of soluble organometallic compounds in supercritical carbon dioxide (sc CO₂) to yield high-purity deposits. Hydrogen, which is miscible with sc CO₂, is typically used as a reducing agent. Recently, we demonstrated the utility of this approach for the deposition of Pt, Pd, Au, and Rh films on planar surfaces (2–4). These reports indicate that pure, continuous films can be deposited at low temperatures (40° to 80°C) using precursors that produce comparatively benign effluents. Whereas this advance addressed the issues of thermal budget and environmental acceptability, planar films similar to those deposited in these examples can be obtained by conventional methods, including chemical vapor deposition (CVD) and line-of-sight techniques such as sputtering. Here, we report the deposition of device-quality Cu and Ni films for use in interconnect and data storage applications, respectively. For Cu, we developed a cold-wall reactor in which metal deposition occurs exclusively on the heated substrate. Moreover, we demonstrate that the conditions used yield unprecedented step coverage that can not be achieved via CVD or physical vapor deposition techniques under practical conditions and can provide filling of sub-100-nm, high-aspect-ratio features in a single step.

The benefits of CFD are a consequence of the physicochemical properties of supercritical fluids (SCFs), which lie intermediate between those of liquids and gases. Consequently, CFD can be viewed as a hybrid of solution plating and vapor phase techniques. Table 1 compares the deposition conditions for each. Like electroless plating, CFD is solution-based, but the transport properties of SCFs, which are more akin to those of a gas, afford distinct advantages that are typically associated with CVD including low viscosity, rapid diffusion, and the absence of surface tension. These properties, when combined with the miscibility of H₂ with sc CO₂, alleviate the sluggish mass transfer typical of liquid-phase reductions and promote conformal coverage. The enabling distinction between CFD and CVD is the mode of precursor transport. In CVD, the limited volatility of suitable precursors, including organometallics, leads to low-vapor-phase concentrations and mass transfer-limited reactions that preclude uniform depositions. In CFD, precursor concentrations in sc CO₂ solution are up to three orders of magnitude greater.

Presently, Cu interconnects are fabricated using a two-step, dual damascene process.

First, a continuous Cu seed layer is deposited within the feature using physical vapor deposition (PVD). This seed layer is then used as a cathode for electrolytic Cu deposition, which fills the trench. Because PVD (sputtering) is essentially a line-of-sight technique, difficulties are encountered when attempting to deposit uniform seed layers in confined geometries. In principle, CVD could be used for this purpose, but to date it has not been successfully integrated. A primary obstacle is precursor volatility constraints, which lead to low-vapor-phase concentrations, mass transport-limited depositions, and ultimately, poor step coverage.

Copper was deposited during CFD by the reduction of CO₂ solutions of either Cu(I) or Cu(II) organometallic compounds in a high-

pressure cold-wall reactor (5). The substrate was placed on a resistively heated stage and maintained at an elevated temperature relative to the bulk solution. At substrate temperatures of 200°C or less, deposition by H₂ reduction of the Cu(II) (betadiketonates), Cu(II) bishexafluoroacetylacetonate [Cu(hfac)₂], and Cu(II) tetramethylheptanedionate [Cu(tmhd)₂] occurred only on the heated stage and was selective for metal surfaces or metal oxide surfaces seeded with catalytic clusters over the bare oxide. For example, H₂ reduction of 0.7 weight percent (wt%) Cu(hfac)₂ solutions in CO₂ at substrate temperatures between 175° and 200°C and a pressure of 200 atm (20.27 MPa) proceeded readily on Ni films or on silicon wafers seeded with small Pd clusters deposited by CFD, but not on the native oxide

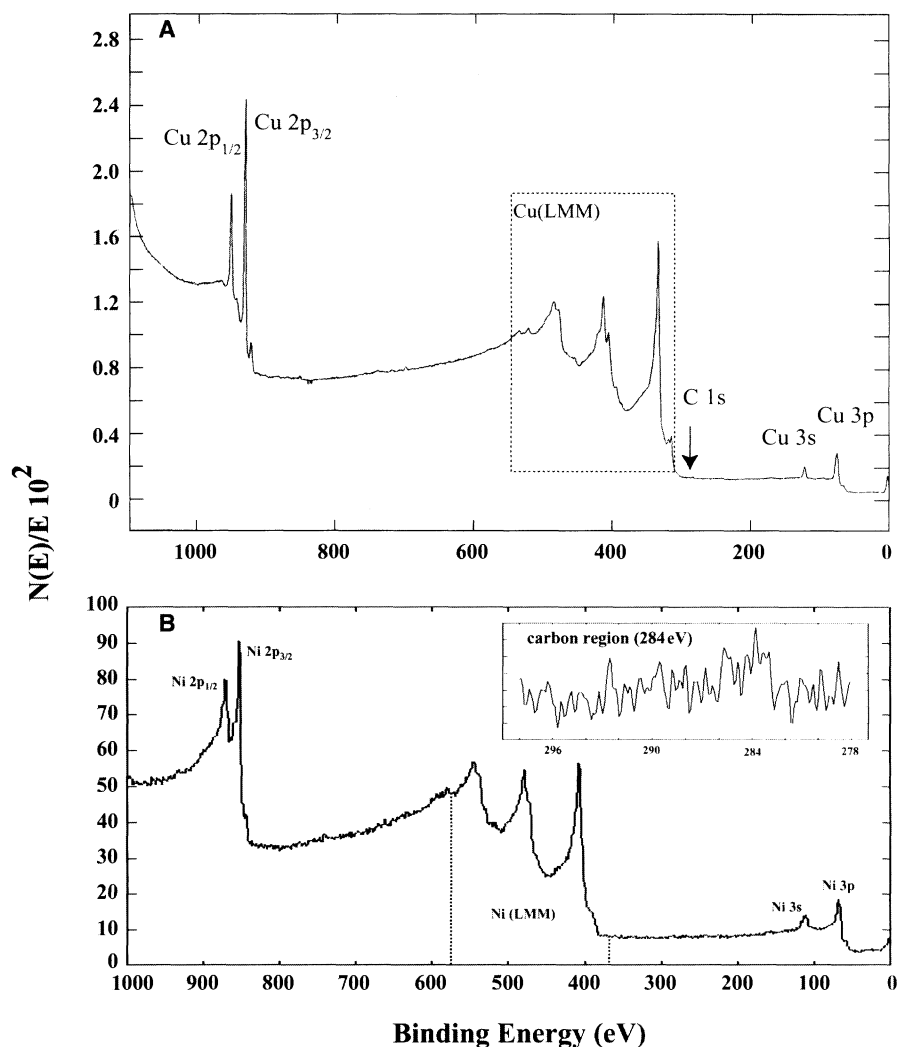


Fig. 1. XPS analysis of metal films deposited by chemical fluid deposition conducted after Ar⁺ sputtering to remove atmospheric contaminants. **(A)** Analysis of a Cu film deposited onto Ni-seeded Si at 200°C by the reduction of Cu(hfac)₂ with H₂ in CO₂ solution in a cold-wall reactor reveals Cu peaks at the appropriate binding energies. There is no significant C contamination (C 1S binding energy = 284 eV). **(B)** Characterization of a Ni film deposited onto glass (60°C) by the co-reduction of NiCp₂ (0.2 wt%) with H₂ and CpPd(C₄H₇) (0.02 wt%) in CO₂ solution reveals Ni peaks at the appropriate binding energies. There is no significant C contamination. Characteristic peaks for Pd at 335 and 340 eV were not observed until additional Ar⁺ sputtering exposed a Pd-rich region adjacent to the substrate surface.

REPORTS

of a Si wafer. This approach affords opportunities for selective film growth through control of the spatial distribution of the seed layer.

In all cases, the deposited films are continuous, highly reflective, and essentially free of impurities. X-ray photoelectron spectroscopy (XPS) indicates insignificant C or F contamination of a Cu film deposited on Ni from $\text{Cu}(\text{hfac})_2$ (Fig. 1A). High purity is facilitated by the high solubility of the ligand by-products in *sc* CO_2 . In fact, F nuclear magnetic resonance (NMR) analysis of the reaction products isolated from the reactor effluent reveals a single peak at ~ 77 parts per million that corresponds to hexafluoropentanedione, which suggests the reduction proceeds cleanly at 200°C with no detectable ligand fragmentation. In addition to promoting film purity, intact desorption of precursor decomposition products provides opportunities for ligand recovery and recycle.

Although deposition from $\text{Cu}(\text{hfac})_2$ yields high-purity films, the presence of F

is undesirable because of environmental and device performance concerns. Because transport in CFD occurs in solution, non-fluorinated precursors that exhibit insufficient vapor pressure for use in CVD are suitable for CFD. For example, deposition from $\text{Cu}(\text{tmhd})_2$ in H_2/CO_2 solutions proceeded readily to yield pure Cu films. Secondary ion mass spectrometry (SIMS) analysis of such a film deposited onto Pd-seeded, etched Si at a substrate temperature of 200°C reveals C and O concentrations of less than 0.2 atomic percent (at%) in the bulk of the film. Further analysis reveals that the high reagent concentrations and favorable fluid-phase transport properties inherent to CFD facilitate conformal deposition. Figure 2A shows a scanning electron microscope (SEM) image of the film cross-section that demonstrates excellent step coverage in narrow (~ 100 nm by 800 nm) trenches. The sample cross-section was prepared using a focused ion beam (FIB).

It is highly desirable to eliminate the seed layers and deposit high-purity, conformal films in a single step. Presently, no such single-step process exists for Cu interconnect metallization. Using CFD, we deposited Cu films directly onto the native oxide of Si at 250°C and onto Cu diffusion barriers such as TiN at slightly lower temperatures by H_2 reduction of $\text{Cu}(\text{tmhd})_2$. SIMS analysis of a 380 -nm-thick film deposited from $\text{Cu}(\text{tmhd})_2$ at 225°C onto TiN indicates that C and O concentrations in the bulk of the films are less than 0.5 at%. The resulting film had low resistivity (~ 2.0 microhm-cm) after annealing, which approaches that of bulk Cu (1.7 microhm-cm) and is well below the upper limit for interconnect structures specified by the ITRS (2.2 microhm-cm) (1).

High-purity Cu films were also deposited in a single step via CFD of Cu(I) compounds of the general type $(\beta\text{-diketonate})\text{CuL}_n$, where L is a Lewis base, and n is 1 or 2. These compounds are known to undergo ther-

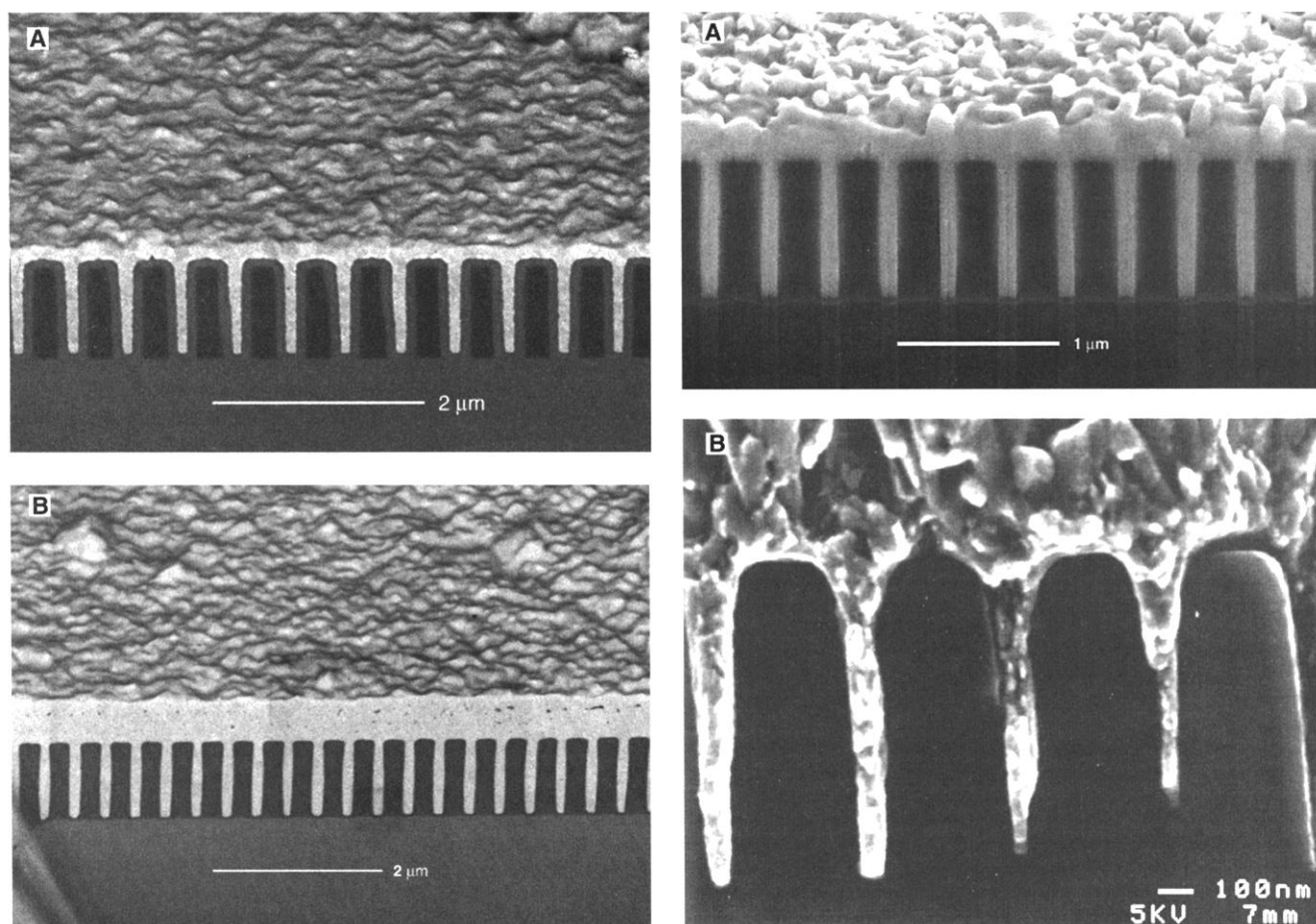
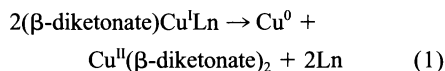


Fig. 2. (Left) FIB SEM micrographs of Cu films deposited by CFD onto (A) a Pd-seeded test wafer by hydrogen reduction of $\text{Cu}(\text{tmhd})_2$ in CO_2 solution at a substrate temperature of 200°C and a pressure of 207 atm and (B) onto a bare Si test wafer by hydrogen-assisted reduction of $\text{Cu}(\text{hfac})(2\text{-butyne})$ in CO_2 solution at a substrate temperature of 225°C and a pressure of 200 atm. Both depositions were conducted in a cold-wall high-pressure reactor. **Fig. 3. (Right)** SEM micrographs of Ni films deposited onto etched Si wafers by the hydro-

gen reduction of NiCp_2 in CO_2 solution in a hot-wall continuous-flow reactor. (A) A FIB SEM image of a film deposited at 60°C and 140 atm provides evidence of a narrow seam within the trenches, indicating uniform film growth from opposing feature surfaces. (B) An SEM image of a fracture cross section of a Ni film deposited conformally at 60°C and 180 atm on a test wafer containing features as narrow as 45 nm that were not etched completely during wafer fabrication (far right).

mal disproportionation during CVD to yield Cu metal and the corresponding Cu(II)(β-diketonate)₂ without the addition of an external reducing agent (Eq. 1) (6)



We deposited high-purity Cu films onto the native oxide of Si wafers as well as Cu diffusion barriers including TiN by hydrogen-assisted reduction of Cu(hfac)(2-butyne) in CO₂ solution at substrate temperatures of 225°C and a pressure of 200 atm. Here, the disproportionation reaction provides a pathway for the initial Cu deposits, which in turn yield active surfaces for H₂ reduction of Cu(hfac)₂ generated by the decomposition of the Cu(I) precursor. This scenario allows for higher deposition efficiency relative to that of the disproportionation reaction alone, because Cu(hfac)₂ generated in situ is also reduced to yield Cu. XPS analysis of films deposited from Cu(hfac)(butyne) yields results similar to that for Cu(hfac)₂. SIMS analysis indicates F contamination is of the order of 1 at%, whereas C and O concentrations are less than 0.5 at%. Figure 2B is a FIB SEM image of a Cu film deposited onto an etched Si wafer from a CO₂ solution of Cu(hfac)(butyne) at 225°C. Step coverage is exceptional despite the presence of a number of trenches that are considerably more narrow at the entrance (<100 nm) than the midpoint. The trench asymmetry is a consequence of wafer preparation prior to metallization. The depositions are not yet optimized, but resistivity of films deposited from Cu(I)(hfac)(2-butyne) in initial experiments is about 2.7 microhm-cm, which is typical of films deposited by CVD. At substrate temperatures of 200°C or less, we find the deposition is selective for metal surfaces including Pt, Pd, and Ni over the native oxide of Si wafers.

The deposition of Ni is of interest for the fabrication of contacts in microelectronic devices and for data storage applications. CFD deposition of Ni from sc CO₂ solutions of bis(cyclopentadienyl)nickel (NiCp₂) proceeds readily at 60°C and 200 atm in the presence of H₂ over Ni, Pd, or Pt films. Low-temperature plating on noncatalytic sur-

faces such as polymers or metal oxides is accomplished by seeding the deposition.

We deposit Ni in batch or continuous hot-wall reactors at 60°C using two strategies (7, 8). The first involves the use of a Pd-seed layer in the same manner as used for the Cu depositions. In the second, solutions of NiCp₂ and an easily reduced organopalladium compound such as 2-methylallyl(cyclopentadienyl)Pd(II) [CpPd(C₄H₇)] are prepared in stoichiometric ratios ranging from 0.005:1 to 0.1:1 (Pd:Ni). The reduction of CpPd(C₄H₇) proceeds immediately in CO₂ upon the addition of H₂ (9) to yield catalytic clusters that serve as nucleation sites for the reduction of NiCp₂. Once the incipient metal surface is formed, growth of the Ni film proceeds readily. This scenario is confirmed by composition analysis by XPS depth profiling, which reveals a Pd-rich Ni deposit at the substrate-metal film interface that is overlain by a pure Ni film. At temperatures above 120°C, Ni can be deposited nonselectively by reduction of NiCp₂/CO₂ solutions without the need for a seed layer or co-reduction with an organopalladium reagent. In all cases, the reduction of NiCp₂ proceeds to completion to yield only the relatively benign hydrocarbon decomposition products and Ni metal. The metal coatings prepared by CFD are reflective, continuous, and free of contamination (10).

Deposition of Ni onto patterned Si wafers is highly conformal. Figure 3 shows SEM micrographs of films deposited within trenches of etched Si wafers from solutions of NiCp₂ using the continuous-feed hot-wall deposition process. Figure 3A is a FIB SEM image of a film deposited onto a Pd-seeded Si wafer at 60°C and 180 atm. The narrow seams in the 100-nm-wide by 800-nm-deep trenches reveal that film growth occurs uniformly from both sides of the trench. Figure 3B is a SEM image of a fracture cross section of a Ni film grown on a substrate containing 75-nm trenches. In this example, two of the trenches were not etched completely during fabrication of the test wafer and left features as narrow as 45 nm (far right), which are filled upon Ni deposition. The deposited films can be grown to virtually any thickness in the flow reactor. For example, we have grown 2.5-μm-thick Ni films that uniformly fill 450 nm wide trenches in etched Si wafers.

Although we have focused on the utility of CFD for device fabrication, the use of nonfluorinated precursors eliminates emission problems typically associated with CVD and the use of CO₂ as the deposition medium obviates the need for aqueous plating baths used for electrolytic and electroless plating that generate large amounts of contaminated wastewater. This is particularly acute for Ni plating: due to large volumes and environmental and human toxicity, nickel is one of 17 high-priority pollutants targeted by the U.S. Environmental Protection Agency for reduction under its 33/50 program (11).

References and Notes

- Semiconductor Industry Association, "1999 International Technology Roadmap for Semiconductors" (Semiconductor Industry Association, San Jose, CA 1999).
- J. J. Watkins, T. J. McCarthy, U.S. Patent 5,789,027 (1998).
- J. J. Watkins, J. M. Blackburn, T. J. McCarthy, *Chem. Mater.* **11**, 213 (1999).
- D. P. Long, J. M. Blackburn, J. J. Watkins, *Adv. Mater.* **12**, 913 (2000).
- All Cu depositions were conducted in a dual flange cold-wall reactor in batch mode. The stainless steel reactor has a total volume of 70 ml and contains a resistively heated stage. Precursor and a single substrate were loaded into the reactor. The vessels were sealed, purged, and charged with CO₂ using a high-pressure syringe pump. The substrate was heated to the desired temperature (typically 200° to 250°C) and the reactor walls were maintained at a lower temperature (typically 60° to 80°C). Film deposition was initiated by the addition of excess of H₂ using a small, pressurized manifold (70 ml). The quantity of H₂ admitted into the vessel was calculated using the pressure-drop measured in the manifold.
- M. Hampden-Smith, T. Kodas, in *The Chemistry of Metal CVD*, T. Kodas, M. Hampden-Smith, Eds. (VCH, New York, 1994).
- All batch depositions were conducted in 17-ml high-pressure stainless steel reactors. A single substrate (~1 cm by 7 cm) and a known amount of precursor were loaded at ambient conditions. The vessels were sealed, purged with CO₂, weighed, placed in a thermal bath, and allowed to equilibrate to the desired temperature. Carbon dioxide was then added to the desired pressure via a high-pressure syringe pump. Film deposition was initiated by the addition of excess of H₂ using a small, pressurized manifold (3.6 ml). The quantity of H₂ admitted into the vessel was calculated using the pressure-drop measured in the manifold.
- Continuous depositions were conducted in a 1.3 cm i.d. by 10.2 cm long hot-wall reactor operating at 60°C and 180 atm. Three computer-controlled high-pressure syringe pumps were used to meter reagent and carrier gas streams to the reactor. The precursor feed stream was either admitted directly to the reactor or was diluted with pure CO₂ upstream of the reactor inlet. Deposition was initiated by metering a ~2 mol% solution of H₂ in CO₂ into the vessel at the desired flow rate. After dilution by all streams, the concentration of precursor at the reactor inlet was approximately 0.2 wt.%. The reactor effluent was directed to an activated carbon bed before venting. Prior to Ni deposition, the substrates were seeded by Pd deposition via hydrogenolysis of CpPd(C₄H₇) in CO₂ solution.
- J. M. Blackburn, D. P. Long, J. J. Watkins, *Chem. Mater.* **12**, 2625 (2000).
- XPS analysis of a film co-deposited at 60°C and 140 atm from a CO₂ solution of NiCp₂ and CpPd(C₄H₇)

Table 1. Comparison of reduction media for the deposition of metal films.

Parameter	Phase		
	Liquid	SCF	Gas (CVD)
Density (g/cm ³)	1	0.1–1	10 ⁻³
Viscosity (Pa · s)	10 ⁻³	10 ⁻⁴ –10 ⁻⁵	10 ⁻⁵
Diffusivity (cm ² /s)	10 ⁻⁵	10 ⁻³	10 ⁻¹
Surface tension (dynes/cm)	20–50	0	0
Precursor conc. (M/cm ³)	10 ⁻³	10 ⁻⁵	10 ⁻⁸
Deposition temp. (°C)	25–80	40–250	250+

(0.2 and 0.02 wt%, respectively) onto glass in a batch reactor reveals Ni peaks at their appropriate binding energies and insignificant levels of carbon contamination (Fig. 1B). Films of similar purity are obtained when Ni depositions are performed on Pd-seeded substrates.

11. U.S. Environmental Protection Agency (EPA) "International Waste Minimization Approaches and Policies

to Metal Finishing," EPA530-R-96-008 (EPA, Washington, DC, 1996).

12. Funded by the NSF (CTS-9734177), the David and Lucile Packard Foundation, and Novellus Systems. We also acknowledge Novellus Systems for assistance with film characterization and donation of test wafers. Facilities supported by the Materials Re-

search Science and Engineering Center at the University of Massachusetts were used for deposit characterization.

6 July 2001; accepted 29 August 2001
Published online 13 September 2001;
10.1126/science.1064148

Include this information when citing this paper.

Organic Carbon Composition of Marine Sediments: Effect of Oxygen Exposure on Oil Generation Potential

Yves Gélinas,^{1*}† Jeffrey A. Baldock,² John I. Hedges¹

Anaerobic sedimentary conditions have traditionally been linked to the generation of the source rocks for petroleum formation. However, the influence of sedimentary redox conditions on the composition of freshly deposited organic matter (OM) is not clear. We assessed the effect of in situ exposure time to oxic conditions on the composition of OM accumulating in different coastal and deep-sea sediments using solid-state ¹³C nuclear magnetic resonance (NMR). ¹³C NMR spectra were resolved into mixtures of model components to distinguish between alkyl carbon present in protein and nonprotein structures. There is an inverse relation between the length of exposure to oxic conditions and the relative abundance of nonprotein alkyl (alkyl_{NP}) carbon, whose concentration is two orders of magnitude higher in coastal sediments with short exposure times than in deep-sea sediments with long exposure times. All alkyl_{NP}-rich samples contain a physically separate polymethylene component similar in composition to algaenans and kerogens in type I oil shales. The duration of exposure to oxic conditions appears to directly influence the quality and oil generation potential of OM in marine shales.

Sedimentary burial of a small fraction [$<0.5\%$ (1–3)] of organic matter (OM) produced in the surface ocean is responsible for the generation of fossil fuels over geologic time scales (4–5). Although the major precursors of these fuels are well characterized within the diagenetic continuum ranging from phytoplankton (6–8) to kerogens (9–14), the variables that control selective preservation of these "protofuels" are still debated (15–17). Oxygen-limited margin environments have long been associated with petroleum source rock formation (4) and, more recently, enhanced OM concentrations (3) and burial efficiencies (16). Yet the link between oxygen levels and the transformation of recently deposited OM into hydrogen-rich petroleum-forming kerogens is not clear. The elucidation of

this link requires studies on organic carbon (OC) compositions in sediments with contrasting oxygen exposure histories. Unfortunately, such studies are hampered, because most OM in marine sediments cannot be characterized at the molecular level (2).

The extent of OM preservation in marine sediments appears to reflect the average period during which accumulating particles are exposed to oxic sedimentary conditions (15, 16, 18). The oxygen exposure time (OET) corresponds to the depth of O₂ penetration into pore waters divided by sediment accumulation rate (3). Such an "oxygen effect" is explained by the lower degradation rate exhibited by recalcitrant macromolecules [such as pollen (19), lignin (20), cutin (13), hydrocarbons (21), and algaenans (7, 8, 12)] under anoxic as compared with oxic conditions. These molecules can be selectively preserved during anoxic diagenesis and generate fuels after thermal catagenesis (4, 13). The oil generation potential of kerogens in marine shales may be determined at the first stage of diagenesis (22) and thus coupled to OET. If this hypothesis is valid, OM from recent diagenetically stabilized sediments with short OETs should be enriched in alkyl functional groups relative to OM from sediments with long OETs.

To test this hypothesis, we developed a demineralization method (23) designed to concentrate OM from marine sediments and used solid-state ¹³C nuclear magnetic resonance (NMR) (24) to compare the chemical compositions of bulk OM in 15 marine sediments representing a wide range of mineralogies and oxygen exposure histories (Table 1). These samples include an OC-rich sulfidic Black Sea sediment (sample 1) and OC-rich sediments from O₂-deficient zones (ODZs) along the Indian (sample 2), Peruvian (sample 3), and Mexican coasts (samples 4 and 5), as well as below (sample 6) and above (sample 7) the Mexican ODZ. Also included are sediments from the Arabian Sea (samples 8 and 9), which exhibits a productivity-driven seasonal pattern of O₂-deficient waters; typical margin deposits accumulating below oxygenated waters on the Washington shelf (sample 10) and upper slope (sample 11); and organic-poor sediments from the Washington coast Cascadia basin (sample 12), Southern Ocean (sample 13), and equatorial Pacific Ocean (samples 14 and 15). This sample set comprises nearshore clastic sediments and carbonate and siliceous oozes, as well as pelagic red clay sediments. $\delta^{13}\text{C}$ and elemental measurements suggest that OM accumulating at these sites is predominantly marine-derived (3).

Major resonances corresponding to alkyl carbon [0 to 45 parts per million (ppm)] dominate all cross-polarization/magic angle spinning (CP/MAS) ¹³C NMR spectra (Fig. 1), with varying contributions from *N*-alkyl/methoxyl (45 to 60 ppm), *O*-alkyl (60 to 95 ppm), di-*O*-alkyl (95 to 110 ppm), aromatic/olefinic (110 to 145 ppm), phenolic (145 to 165 ppm), and carboxyl/amide (165 to 190 ppm) carbon. The seven organic-rich samples (Fig. 1, A through C) exhibit similar intensities within these chemical shift regions. Although variations in the relative contribution of each type of carbon increase among the five samples with intermediate OC concentrations (Fig. 1, D through F), resonance shapes and chemical shift values at maximum resonance intensity are similar to those obtained for organic-rich samples. Such variations between, rather than within, the different types of carbon functionalities may reflect mixtures of similar components at varying proportions. In contrast, spectra obtained for samples with low OC concentrations show greater variation in resonance shapes and relative intensities (Fig. 1, G through I). The

¹School of Oceanography, Box 357940, University of Washington, Seattle, WA 98195-7940, USA. ²Commonwealth Scientific and Industrial Research Organization (CSIRO) Land and Water, Personal Mail Box 2, Glen Osmond, South Australia 5064, Australia.

*To whom correspondence should be addressed.

†Present address: Department of Chemistry and Biochemistry, Concordia University, 1455 de Maisonneuve Boulevard West, Montreal, Quebec, Canada, H3G 1M8. E-mail: ygelinas@alcor.concordia.ca